J Mater Sci (2023) 58:15676–15695

Composites & nanocomposites

Enhancing curing, mechanical and electrical properties of epoxidized natural rubber nanocomposites with graphene and carbon nanotubes hybrid fillers

Thananya Siriwas[1], Skulrat Pichaiyut[1], Markus Susoff[2], Svea Petersen[2], and Charoen Nakason[1,*]

[1] *Faculty of Science and Industrial Technology, Prince of Songkla University, Surat Thani Campus, Surat Thani, Thailand*
[2] *Faculty of Engineering and Computer Science, University of Applied Sciences Osnabrück, Osnabrück, Germany*

Received: 3 July 2023
Accepted: 30 September 2023
Published online: 24 October 2023

ABSTRACT

The effect of incorporating a combination of hybrid carbon fillers, graphene (GP), and carbon nanotubes (CNT) into epoxidized natural rubber with 25 mol% epoxidations (ENR-25) nanocomposites was investigated. The results demonstrated significant effects of CNT incorporation in ENR-25/GP–CNT hybrid composites on the cure characteristics, including shorter scorch and cure times, lower activation energy, and higher torque difference as the CNT loading increased. Fourier Transform Infrared analysis revealed a decrease in absorption intensity at a wavenumber of 1115 cm^{-1} with increasing CNT loadings. This observation can be attributed to chemical interactions between the polar functional groups in the ENR molecules and the polar groups on the CNT surfaces. Additionally, the hybrid GP–CNT filler was found to improve the mechanical properties, such as modulus and hardness, of the ENR/GP–CNT hybrid composites. The crosslink densities of the hybrid composites were measured using the Flory–Rehner theory, showing an increasing trend with higher CNT loadings. This phenomenon can be explained by the formation of end-to-end connections between certain parts of the CNT and the GP, leading to the establishment of a three-dimensional filler network with strong interactions among the components. Consequently, this facilitates the good dispersion and distribution of CNT within the composites. The observed trends in the mechanical properties were consistent with an increasing Payne effect and electrical conductivity as the CNT loadings increased. Notably, it was found that the ENR/GP–CNT hybrid composites exhibited a low percolation threshold concentration of 2.34 phr of CNT, indicating that they behave as conductive rubber materials.

Handling Editor: Gregory Rutledge.

Address correspondence to E-mail: charoen.nakason@gmail.com

https://doi.org/10.1007/s10853-023-09003-3

Introduction

Epoxidized natural rubber (ENR) has garnered significant interest among researchers as a modified derivative of natural rubber (NR) with a higher degree of polarity and other related properties. ENR is commonly produced through the in situ epoxidation of NR using formic acid and hydrogen peroxide [1]. The degree of epoxidation in ENR is typically regulated by manipulating the molar ratio of NR and peracid, the reaction time, and temperature. The inclusion of the epoxirane (or epoxide) rings has a substantial impact on the properties including superior oil resistance, thermal stability, weathering resistance, and electrical conductivity compared to unmodified NR [2]. However, ENR still maintains the exceptional properties of NR, including its ability to undergo strain-induced crystallization, resulting in excellent mechanical and dynamic properties [3]. In addition, ENR can be crosslinked by various chemicals such as di- and multifunctional group substances, including amines [4], anhydrides [5], and carboxylic acids [6].

The active carbon filler particles with polar functional groups at their surfaces have been widely utilized to enhance polymer composite properties [7]. These fillers include carbon black (CB), graphite (G), conductive carbon black (CCB), carbon nanotubes (CNT), and graphene (GP). Although they share the same chemical compositions, the variations in their structures give rise to distinct enhancement characteristics. These structural differences play a crucial role as multifunctional additives in elastomeric materials enhancing several important properties. One notable example is the synergistic effect achieved by combining CNT and GP, which can significantly enhance the electrical conductivity of styrene butadiene rubber (SBR) [8]. Moreover, the incorporation of CNT and graphene oxide (GO) into natural rubber (NR) composites has been shown to induce the formation of complex filler networks, resulting in enhanced tensile strength, 100% modulus, and tear strength [9]. Similarly, the homogeneous dispersion of multi-walled carbon nanotubes (MWCNT) and GP nanofillers in silicone rubber (VMQ) has demonstrated a synergistic improvement in tensile strength, Young's modulus, and glass transition temperature of the hybrid composite. This improvement can be attributed to the fine dispersion of the MWCNT-GP hybrid filler within the VMQ matrix, which promotes strong interfacial interaction [10]. Furthermore, the introduction of a CNT-GP hybrid filler into nitrile rubber (NBR) has been investigated, revealing significant enhancements in the mechanical properties of the material [11].

Graphene (GP) is a two-dimensional (2D) material consisting of a single layer of carbon atoms bonded together by covalent bonds with sp^2 hybridized carbon structures [12]. The aspect ratio of GP varies depending on its width-to-thickness ratio. GP exhibits remarkable physical properties, including a high specific surface area (SSA), excellent light transmittance across a broad range of wavelengths [13], exceptional mechanical strength [14], flexibility [15], high carrier mobility [16], thermal conductivity [17], and outstanding electrical conductivity [18]. Mixing GP and other carbon fillers with rubber typically result in the formation of agglomerations due to strong Van der Waals interactions among the filler particles. These agglomerations adversely affect both mechanical properties and the formation of conductive pathways. It has been reported that the dispersion of fillers can be improved by introducing a secondary filler to create hybrid fillers [19]. One promising option for a secondary filler is CNT, which are one-dimensional (1D) derivatives of graphitic carbon allotropes formed by rolling GP into a cylindrical structure [20]. CNT has shown the ability to enhance composite properties, including mechanical strength, electrical conductivity, and thermal stability [21].

In recent years, there has been a growing interest in materials with a three-dimensional (3D) network structure, as they have the potential to enhance both mechanical and electrical properties [22]. However, the formation of a 3D network in a polymer matrix is often hindered by agglomeration, which is typically caused by Van der Waals interactions and even hydrogen bonding among the filler particles [23]. One potential approach to improve filler dispersion and enhance the final composite properties is the hybridization of fillers such as CNT (1D) with graphene platelets (2D) in a 3D structure [24]. This allows for the formation of a three-dimensional hybrid network that not only acts as conducting pathways but also strengthens other relevant properties [23].

The objective of this study was to analyze the effects of incorporating a hybrid filler consisting of GP/CNT (graphene nanoplatelet/carbon nanotubes) with different CNT loadings on the mechanical and electrical properties of ENR nanocomposites. Additionally, the investigation included an examination of the cure characteristics, thermal properties, mechanical

properties, relaxation behavior, crosslink density, electrical properties, and morphological properties of the ENR vulcanizates, along with an analysis of the chemical reactions among the involved components.

Experimental

Materials

Epoxidized natural rubber with 25 mol% epoxide (ENR-25) was manufactured by Muang Mai Guthrie Public Company Limited (Surat Thani, Thailand). Graphene (GP) with a specific surface area of 180 m^2/g, thickness up to 3 nm, and an average particle size of 10–30 μm, with about 99.8% purity, was obtained from Graphene Star Ltd (London, UK). The multi-wall carbon nanotubes (CNT), NC7000, which had a diameter of 9.5 nm, length of 1.5 μm, and 90% purity, were manufactured by Nanocyl S.A. (Sambreville, Belgium). Additionally, other chemicals used in the rubber formulations (Table 1) included cure activators (zinc oxide and stearic acid), a cure accelerator (2,2′-dithiobis benzothiazole, MBTs), and sulfur curing agent were used as received.

Preparation of GP/CNT-filled ENR-25 nanocomposites

The ENR-25 nanocomposites were prepared using a tangential internal mixer, Brabender Plasticorder with Mixer 50 EHT model 835205 (Duisburg, Germany) at 60 °C and a rotor speed of 60 rpm. An optimum loading of 5 phr of GP was compounded [25] with various CNT loadings (0, 1, 3, 5, and 7 phr), represented by ENR-25/GP_5 and ENR-25/GP_5–CNT_x (x is CNT loading), respectively. The compounding process involved first masticating ENR-25 for about 1 min, followed by sequential addition of cure activators (i.e., zinc oxide and stearic acid) with continued mixing for about 2 min. Then, 5 phr of GP was incorporated and mixed for 5 min, resulting in a sample is designated as "ENR-25/GP_5." To prepare ENR filled with GP_5/CNT hybrid filler compounds, the same procedure was followed, but mixing with each loading of CNT was conducted for about 2 min after incorporating GP. Cure accelerator (MBTs) and sulfur were sequential added, and the mixing was continued for another 4 min to reach the total mixing time of 12 min. Gum rubber compound (without filler) was also prepared using the same mixing procedure for a comparison purpose. The rubber compound was then sheeted out through the 1 mm nip of a two-rolls mill, model YFCR 600, Yong Fong Machinery Co., Ltd. (Samut Sakorn, Thailand), repeating for several cycles to improve the dispersion of filler particles in the rubber matrix. The cure characteristics of the rubber compounds were investigated using a moving die rheometer (MDR), model MDR 2000, Alpha Technologies, (Ohio, USA) at 160 °C. Finally, rubber vulcanizate sheets were prepared by a compression molding, model PR1D-W400L450PM, Charoen Tut Co., Ltd, (Samut Prakarn, Thailand) at 160 °C, and the respective cure time based on the MDR test.

Table 1 Material sources and compounding formulation

Materials	Supplier	Amount (phr)
ENR-25	Muangmai Guthrie Co., Ltd., (Surat Thani, Thailand)	100
Stearic acid	Imperial Chemical Industry Co., Ltd., (Pathum Thani, Thailand)	1
Zinc oxide (ZnO)	Global Chemical Co., Ltd., (Samut Prakarn, Thailand)	5
2,2-Dithiobis-(benzothiazole) (MBTs)	Flexsys, (Termoli, Italy)	1
Sulfur (S)	Ajax Chemical Co., Ltd., (Samut Prakarn, Thailand)	2.5
GP	Graphene Star., Ltd., (London, England)	5
CNT	Nanocyl S.A., (Sambreville, Belgium)	1, 3, 5, and 7

Attenuated total reflection Fourier transform infrared spectroscopy (ATR-FTIR)

The ATR-FTIR of ENR-25/GP_5–CNT_x nanocomposites were performed by a Thermo Nicolet Avatar 360 FTIR (Thermo Electron Corporation, Thermo Nicolet, Madison, Wisconsin, USA). The measurements were operated with a resolution of 2 cm^{-1} and over a wavenumber range of 4000–500 cm^{-1}.

Morphological characterization

Morphology of ENR-25/GP_5–CNT_x hybrid nanocomposites was characterized by Transmission Electron Microscope (TEM), JEM 2010, Jeol Ltd., Tokyo, Japan) with an accelerating voltage of 200 kV. The samples were first cut to a thickness of approximately 70 nm by Cryo-Ultramicrotome (RMC, MT-XL) before TEM imaging. Furthermore, scanning electron microscopy (SEM) of ENR-25/GP_5–CNT_x nanocomposites with different CNT loadings (1, 3, 5, and 7 phr) was also conducted by a ZeissSupra-40 VP, Carl Zeiss Microscopy GmbH (Oberkochen, Germany). The rubber samples were firstly cryogenically fractured in liquid nitrogen to create new cross-sectional surfaces and were then sputter-coated with a thin layer of gold under vacuum prior to SEM characterization.

Cure characteristics

The cure characteristics of rubber compounds were assessed using a moving die rheometer, model MDR 2000, Alpha Technologies, (Ohio, USA) at 160 °C for 30 min. The curing curves were then used to determine the optimum scorch time (t_{s1}), cure time (t_{c90}), minimum torque (M_L), maximum torque (M_H), and torque difference (M_H–M_L).

Activation energy of vulcanization

The activation energy for the vulcanization of gum ENR-25, ENR-25/GP_5, and ENR-25/GP_5–CNT_x was determined using a differential scanning calorimeter (DSC), Mettler-Toledo Ltd., (Gießen, Germany). The experiments were carried out over a temperature range of 10–300 °C and heating rates of 2, 10, 20, and 30 K/min.

Mechanical properties

Specimens of vulcanized rubber sheets in a dumbbell shape (type 5A) were firstly created by die cutting, following the guidelines of ASTM D-638. These specimens were then subjected to tensile testing at room temperature, using the testing standard of ISO 527. The tests were conducted using Zwick Z-1545 tensile testing machine, Zwick GmbH & Co., (Ulm, Germany) with extension speed of 200 mm/min and repeated with five specimens for each test. The hardness of the samples was also determined using a Shore A durometer, Frank GmbH, (Hamburg, Germany) following ISO 868. The tension test was performed according to ISO 2285, the samples were kept under tension for a fixed strain of 100% for 10 min, and tension set was calculated as follow [26]:

$$\text{Tension set } (\%) = \frac{L_1 - L_0}{L_0} \tag{1}$$

where L_0 is the initial length (20 mm) before testing, and L_1 is the length after testing.

Crosslink density

In order to analyze the crosslink density and network structure of ENR-25 vulcanizates, the following experimental procedure was conducted. The specimens, with dimensions of 10 × 10 × 2 mm^3, were initially weighed and then immersed in toluene at room temperature for a duration of 7 days. Following the immersion period, the swollen rubber samples were carefully removed and any excess liquid on the specimen surfaces was wiped off. Subsequently, the specimens were dried in a vacuum oven at 40 °C for 24 h. Once the drying process was complete, the swollen samples were weighed again to determine their final weights. The crosslink density was determined by comparing the final weights of the swollen samples to their original weights before immersion. This analysis employed the Flory–Rehner equation [27]:

$$v = \frac{-\text{In}(1 - \emptyset p) + \emptyset p + X \cdot \emptyset_p^2}{V_L \cdot \left(\emptyset_p^{1/3} - \frac{\emptyset p}{2}\right)} \tag{2}$$

In the above equation, the variable v represents the crosslink density (mol/m^3), The volume fraction of rubber in a swollen network is denoted by $\varnothing_p$, while

V_L denotes the molar volume of toluene (106.1 cc/mol for toluene), and ρ_p represents density of the polymer. The Flory–Huggins-interaction parameter of polymer and solvent, X, was assigned a value of 0.4 based on the relevant literature [28].

To calculate the volume fraction of rubber in the swollen network ($\varnothing_p$), the volume fraction of the filler needed to be subtracted. The following equation (Eq. 3) was employed for this purpose:

$$\emptyset p = \frac{1}{1 + \left(\frac{m - m_d}{m_d}\right) \times \frac{\rho_p}{\rho_s}} \tag{3}$$

where m and m_d represent the mass of the swollen sample and the mass of the sample after drying, respectively. ρ_p represents density of the polymer, and ρ_s represents density of the solvent.

It is important to note that Eqs. (2) and (3) are applicable exclusively to unfilled rubber vulcanizate networks. In contrast, in the case of rubber nanocomposites, it becomes imperative to consider the effective reinforcing factor and the filler-rubber interaction, along with the volume fraction of fillers. This consideration is addressed by the following equation [29]:

$$\frac{\emptyset_p}{\emptyset_{rf}} = 1 - \left[3c\left(1 - \emptyset_p^{1/3}\right) + \emptyset_p - 1\right]\left(\frac{\emptyset_f}{1 - \emptyset_f}\right) \tag{4}$$

where $\emptyset_{rf}$ is the volume fraction of filled rubber in swollen gel, $\emptyset_f$ is the volume fraction of filler in the unswollen filled rubber, and c is the filler-rubber interaction parameter.

A new parameter, $\emptyset_p$, introduced in Eq. (4), has been incorporated into the Flory–Rehner equation (Eq. 2) to accommodate the factors of filler–rubber interaction and the volume fraction of filler in the system.

Payne effect

The Payne effect, which is used to evaluate filler dispersion and interactions within rubber compounds, was determined using a rubber process analyzer (RPA), Alpha Technologies (Akron, USA). The relationship between storage moduli and strain amplitude was measured to assess the degree of the Payne effect. This includes interactions between fillers (filler–filler interactions) and between fillers and rubber (filler–rubber interactions) [30]. To conduct the test, the storage shear modulus (G') of each filled un-vulcanized rubber compound was measured under shear deformation. The measurements were performed within a strain amplitude range of 0–100% at a fixed oscillating frequency of 1 Hz and at a temperature of 100 °C. To quantify the level of the Payne effect, the difference between the maximum and minimum shear moduli ($\Delta G'$) was calculated in relation to the minimum storage modulus [31]:

$$\Delta G' = G'_{max} - G'_{min} \tag{5}$$

$$\%\Delta G' = \left(\frac{G'_{max} - G'_{min}}{G'_{min}}\right) \times 100 \tag{6}$$

$$\text{Payne effect } (\%) = \%\Delta G'_{\text{Filled ENR}} - \%\Delta G'_{\text{Gum ENR}} \tag{7}$$

where G'_{max} and G'_{min} are the maximum and minimum storage moduli.

Electrical properties

The electrical conductivity (σ) of ENR-25/GP_5 and ENR-25/GP_5–CNT_x nanocomposites, with varying amounts of CNT (1–7 phr), was measured at room temperature using an LCR meter (Hioki IM 3533, Hioki E.E. Corporation, Nagano, Japan). The LCR meter was connected to the electrode plates of the dielectric test fixture (dielectric test fixture 16451B, Test Equipment Solutions Ltd., Berkshire, United Kingdom), which had an electrode diameter of 5 mm. Prior to the test, a sample with a thickness of approximately 2 mm was placed between the plates. The electrical conductivity (σ) was calculated using the following formula [32]:

$$\sigma = \frac{1}{\rho} = \frac{d}{R_p \cdot A} \tag{8}$$

where d represents the sample thickness, A is the electrode area, ρ is the volume resistivity, and R_p denotes resistance.

Results and discussion

Characterization of ENR-25/GP–CNT hybrid filler by ATR-FTIR

The chemical structure of the rubber nanocomposites developed with hybrid fillers was determined through FTIR analysis, as depicted in Fig. 1, and the

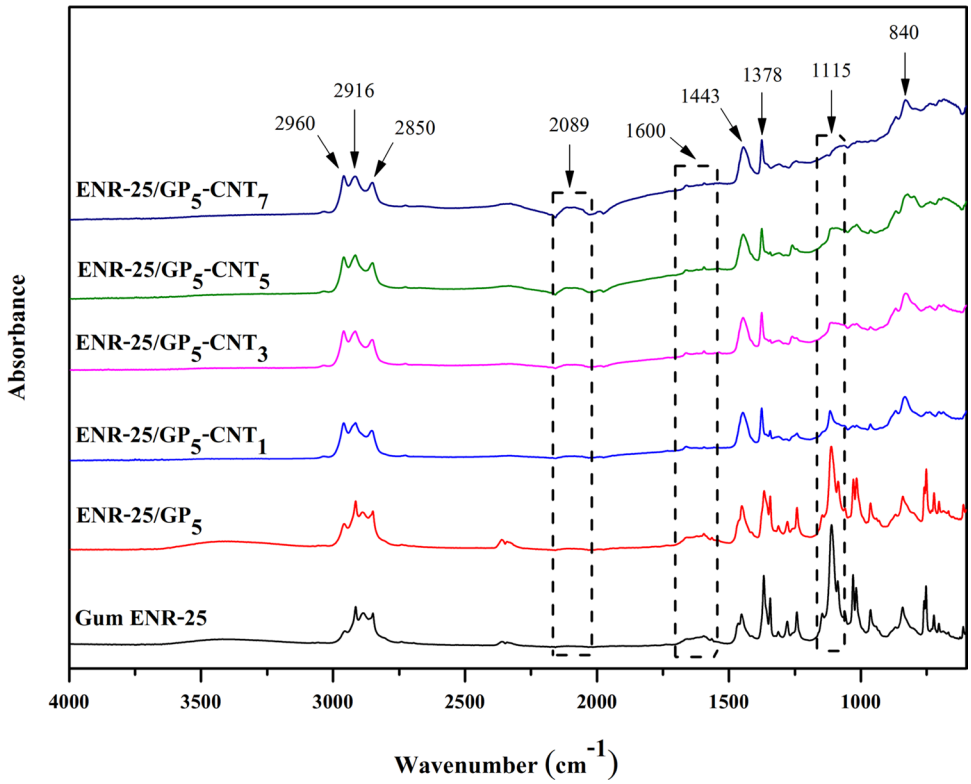

Figure 1 FTIR spectra of gum ENR-25, and its filled compounds with 5 phr of GP (ENR-25/GP_5), and ENR-25/GP_5–CNT_x hybrid nanocomposites with varying CNT loadings at 1, 3, 5, and 7 phr.

Table 2 Assignments of FTIR peak absorptions for gum ENR, ENR-25/GP_5 and ENR-25/GP_5–CNT_x nanocomposites with various CNT loadings at 1, 3, 5, and 7 phr

Wave number (cm^{-1})	Assignments
840	=CH out-of-plane bending vibrations [31]
1115	C–O–C stretching vibration [21]
1378	$–CH_3$ bending vibration [34]
1443	CH scissoring vibration [34]
1600	C=C bending vibration [34]
2850	C–H stretching vibration [35]
2916	C–H stretching vibration [35]
2960	C–H stretching vibration [35]

peak assignment is provided in Table 2 The absorption peaks at 840 cm^{-1} can be attributed to the out-of-plane bending vibrations of =C–H bonds in the isoprene units. Additionally, small peaks observed at 1600 cm^{-1} indicate the C=C bending vibration of the isoprene units. The low intensity of these peaks suggests a limited number of double bonds present in the ENR molecular chains. This is a result of the high concentration of epoxirane groups that have replaced the double bonds in the isoprene units of NR molecules. Moreover, three distinct peaks at wavenumbers 2850, 2916, and 2960 cm^{-1} correspond to C–H stretching vibrations. Furthermore, a notable peak was observed at the wavenumber 1115 cm^{-1}, which represents the C–O–C stretching vibration in the epoxirane ring of ENR molecules. The intensity of this peak (1115 cm^{-1}) was found to decrease with increasing CNT loadings. This can be attributed to the chemical interactions between the polar functional groups in the ENR molecules and the GP or CNT surfaces, as depicted in the proposed reaction mechanism shown in Fig. 2. It suggests that the ring opening reaction of the oxirane rings in the ENR molecule occurs during high-temperature mixing (> 70 °C), resulting in the formation of diol groups on the ENR molecular chains [33]. These groups are capable of further reacting with the –OH and –COOH groups on the GP or CNT surfaces, leading to a decrease in the absorption peak intensity at 1115 cm^{-1}.

Morphological properties

Scanning electron microscope (SEM) and transmission electron microscope (TEM) were employed to examine the morphological properties and network formation of GP and CNT in the ENR-25 matrix, as shown in Figs. 3 and 4, respectively. Figure 3a illustrates that

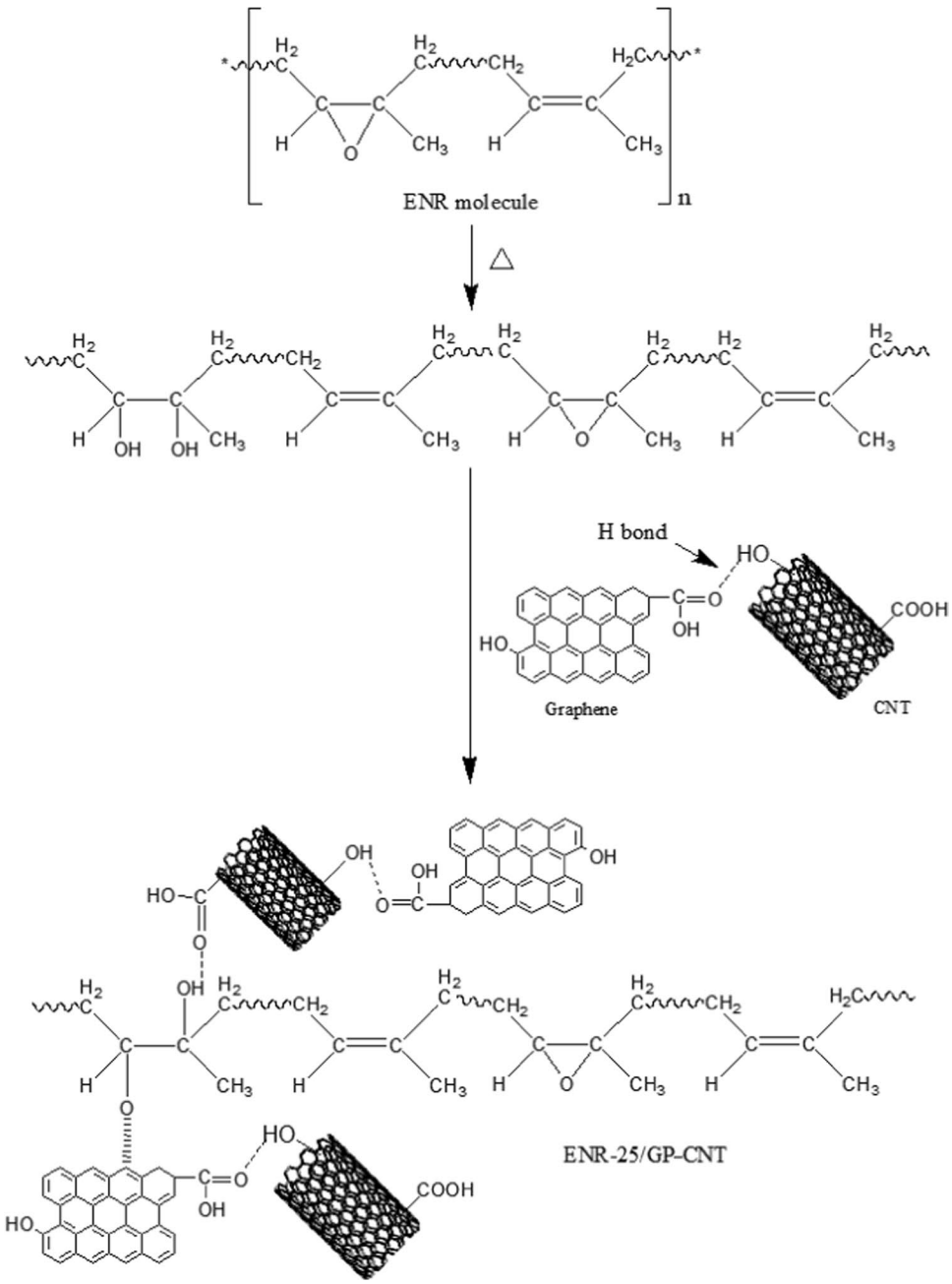

Figure 2 A proposed reaction mechanism of ENR molecules with polar functional groups on graphene nanoplatelets (GP) and carbon nanotubes (CNT) surfaces during the vulcanization process.

in the ENR-25/GP_5 composite, GP appears as overlapping sheets that self-embed in the ENR-25 matrix, along with some interconnected regions. When 1 phr of CNT is combined with 5 phr of GP in the ENR-25 matrix (Fig. 3b), certain parts of the CNT connect with the GP, forming end-to-end connections. This is attributed to the interaction of polar functional groups between the hybrid fillers, resulting in good dispersion and distribution of CNT [36]. This is further confirmed by the TEM images in Fig. 4a, where the homogeneous dispersion and distribution of CNT bundles are clearly observed. Increasing the CNT loading to 3 phr (Fig. 3c) and 5 phr (Fig. 3d) in the ENR-25 matrix leads to further end-to-end connections among CNT bundles and GP, but also the presence of some filler agglomerates due to strong filler–filler interactions (Fig. 2). Furthermore, with an increase in CNT loading to 7 phr, larger filler agglomerates become evident in Fig. 3e, which is also clearly verified in the TEM image in Fig. 4b. This can be attributed to an excessive filler loading

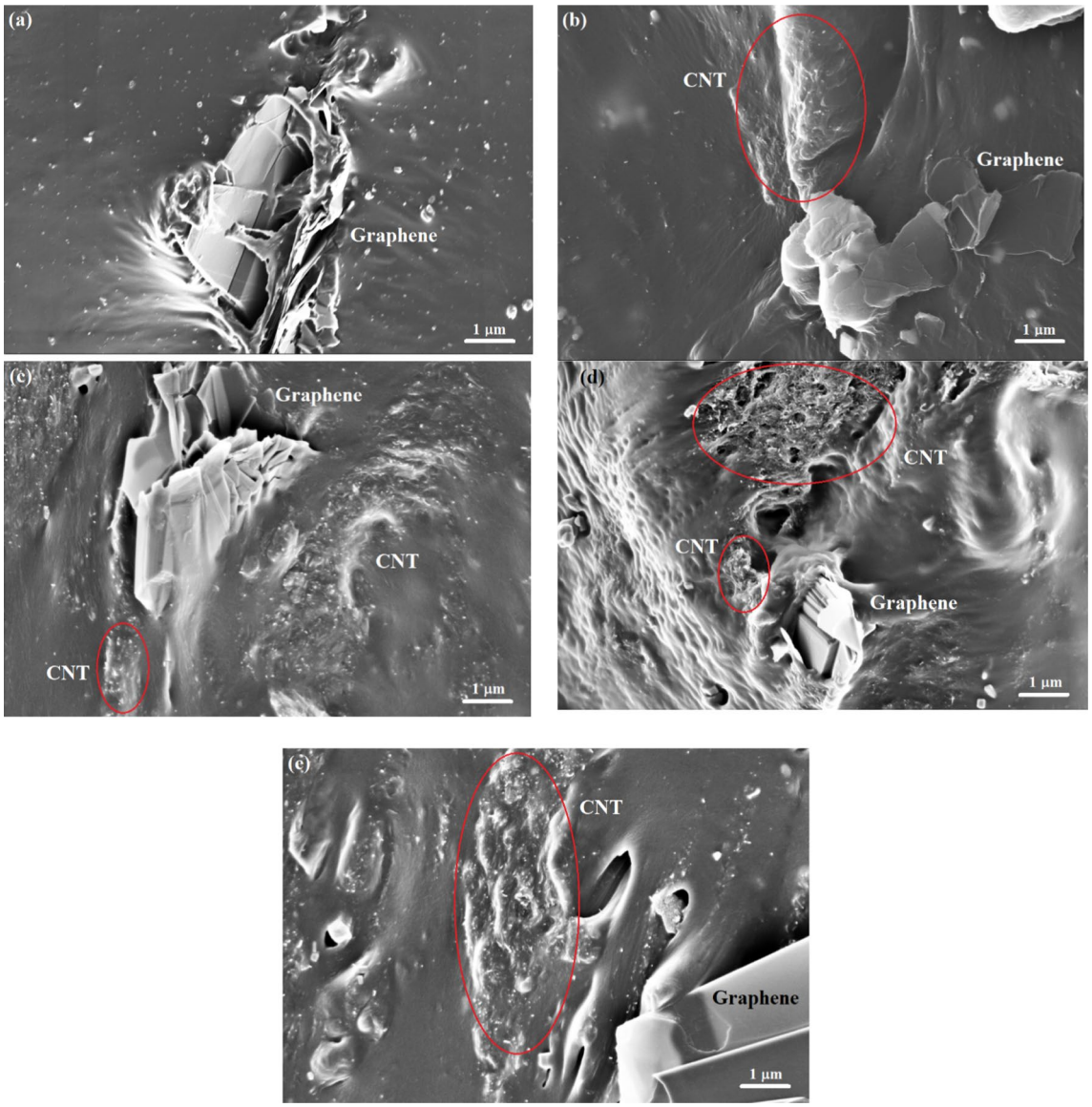

Figure 3 SEM micrographs of a ENR-25 filled with 5 phr of GP (ENR-25/GP_5), and ENR-25/GP_5–CNT_x hybrid nanocomposites with varying CNT loadings at **b** 1 phr, **c** 3 phr, **d** 5 phr, and **e** 7 phr.

that surpasses the filler–polymer interactions based on Van der Waals forces, dipole–dipole interactions, and hydrogen bonding among the filler particles [36].

Cure characteristics

Figure 5 illustrates the influence of CNT dosage on the cure characteristics, with the curing properties summarized in Table 3. It is evident that as the CNT loadings increase, there is a gradual decrease in both the scorch time (t_{s1}) and cure time (t_{c90}). This can be attributed to the high thermal conductivity of CNT [37], which enhances the crosslinking reaction of ENR [38]. Moreover, the presence of oxygen-containing groups (such as hydroxyl and carboxyl groups) on the surfaces of CNT and GP may act as accelerating agents in the crosslinking reaction of ENR. Furthermore, the incorporation of varying CNT loadings into ENR compounds resulted in an increasing trend in the cure rate index (CRI) (Table 3). This is likely due to the enhanced reactivity of the hybrid filler particles through the interaction of polar functional groups with the ENR crosslinking reaction [39]. Additionally, the torque difference (M_H–M_L), which reflects

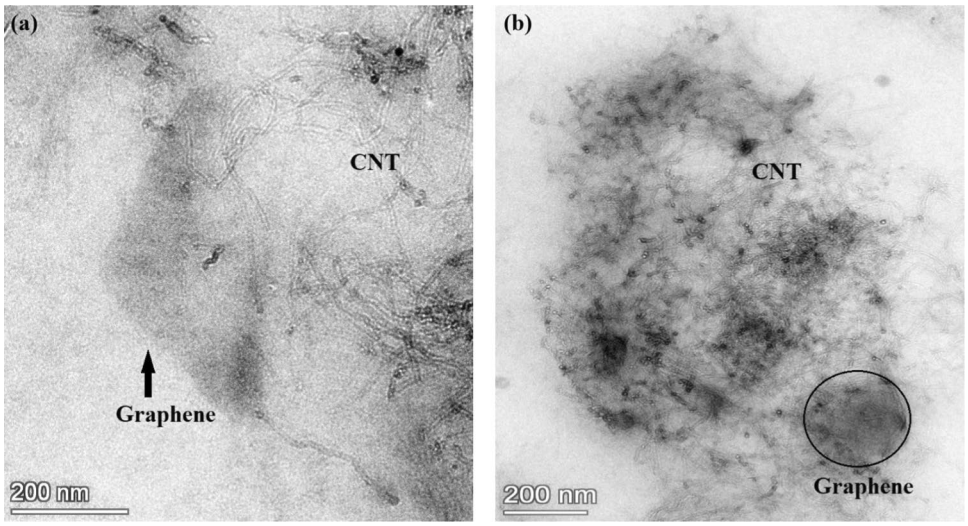

Figure 4 TEM micrograph of ENR-25/GP_5–CNT_x hybrid nanocomposites with different CNT loadings at **a** 1 phr and **b** 7 phr.

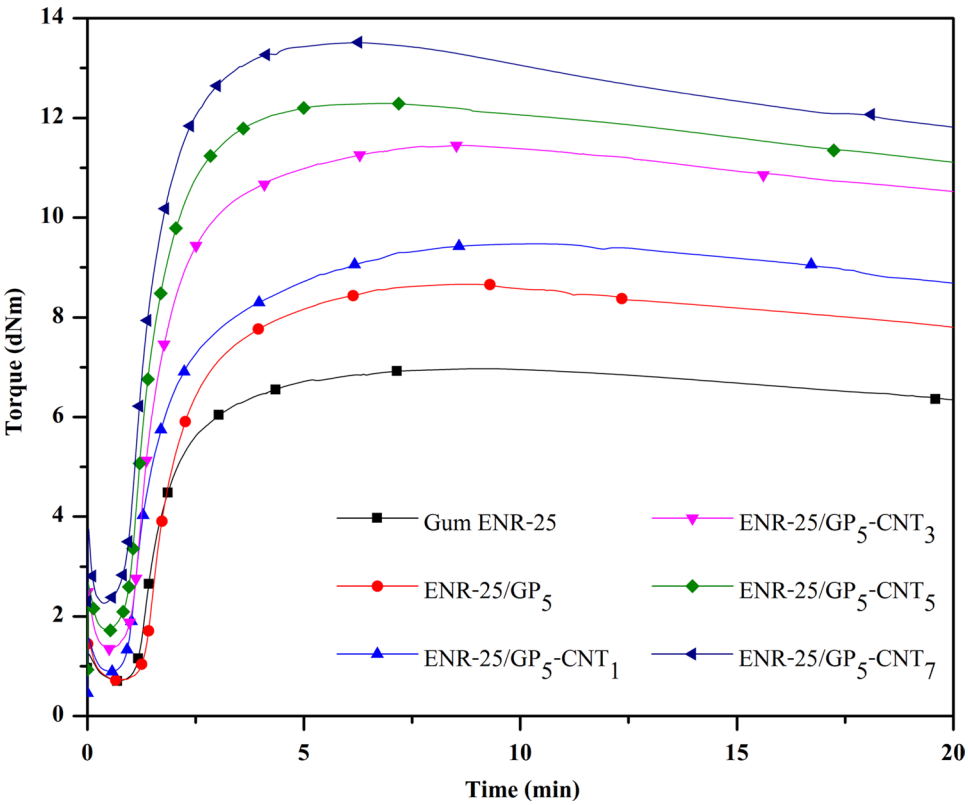

Figure 5 Cure curves of gum ENR-25 and its filled compounds with 5 phr GP (ENR-25/GP_5) and ENR-25/GP_5–CNT_x hybrid nanocomposites with different CNT loadings at 1, 3, 5, and 7 phr.

the crosslink density [40], increased with higher CNT loadings. This can be attributed to the polar functional groups on the surfaces of the hybrid fillers reacting with the epoxide groups of ENR molecules (Fig. 2). As a result, more crosslinked networks are formed, leading to higher crosslink density, as indicated by the increasing trend in torque difference (Table 3). Moreover, the increased amount of particulate filler particles in the rubber matrix restricts the mobility of rubber molecular chains, resulting in increased stiffness, torque difference, and consequently higher crosslink density [41].

The activation energy (E_a) of vulcanization can be determined by analyzing different heating rates of

Table 3 Cure characteristics in terms of minimum torque (M_L), maximum torque (M_H), torque difference (M_H–M_L), scorch time (t_{S1}), cure time (t_{90}), and cure rate index (CRI) for gum ENR compound and its filled compounds with graphene (ENR-25/GP_5) as well as hybrid filler (ENR-25/GP_5–CNT_x) with various CNT loadings

Samples	Cure characteristics					
	M_L (dN m)	M_H (dN m)	M_H-M_L (dN m)	t_{S1} (min)	t_{C90} (min)	CRI* (min^{-1})
Gum ENR-25	0.60	6.98	6.38	1.42	4.78	29.76
ENR-25/GP_5	0.72	8.62	7.90	1.30	3.72	41.32
ENR-25/GP_5–CNT_1	0.89	9.48	8.59	1.02	3.32	43.48
ENR-25/GP_5–CNT_3	1.35	11.46	10.11	1.00	3.21	45.25
ENR-25/GP_5–CNT_5	1.72	12.30	10.58	0.98	2.86	53.19
ENR-25/GP_5–CNT_7	2.26	13.52	11.26	0.92	2.77	54.05

*CRI = $\frac{100}{t_{c90}-t_{s1}}$

the reaction. The Ozawa and Kissinger methods are commonly used to calculate the activation energy of vulcanization using the following equations [42], respectively:

$$E_a = -R\frac{d\ln q}{d\left(\frac{1}{T_p}\right)} \quad (9)$$

$$E_a = -R\frac{d\ln\left(\frac{q}{T_p^2}\right)}{d\left(\frac{1}{T_p}\right)} \quad (10)$$

Here, q is the heating rate, T_p is the temperature of the exothermic peak, and R is the gas constant (8.314 JK^{-1} mol^{-1}).

By applying the Ozawa and Kissinger equations, the relationship between ln q with $1000/T_p$ (Eq. 9) and ln $\left(\frac{q}{T_p^2}\right)$ with $1000/T_p$ (Eq. 10) for various gum and filled ENR-25 compounds can be observed, as depicted in Fig. 6. The activation energy (E_a) of the vulcanization reaction in different ENR-25 compounds with various types of fillers can be determined from the slopes of the straight line plots in Fig. 6, as summarized in Table 4. It is evident that both equations yield lower E_a values with the incorporation and increasing filler loadings. Specifically, the ENR-25/GP_5 composite exhibits a lower E_a compared to the gum ENR-25 compound. Furthermore, the incorporation of CNT in the ENR-25/GP_5 composite to form ENR-25/GP_5–CNT_x composites, as well as increasing CNT loadings, results in decreasing E_a values based on both models (Table 4). This suggests that the

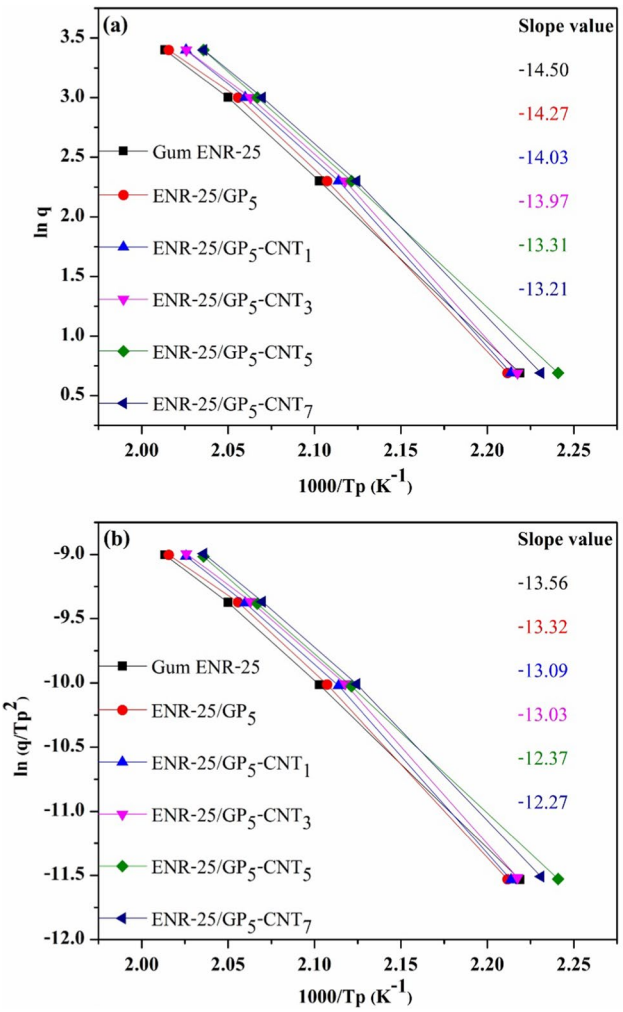

Figure 6 The correlation between heating rate and the temperature of exothermic peak for gum ENR-25 and its filled compounds with 5 phr GP (ENR-25/GP_5) and ENR-25/GP_5–CNT_x hybrid nanocomposites with different CNT loadings at 1, 3, 5, and 7 phr based on **a** the Ozawa and **b** Kissinger equations.

Table 4 The activation energy (E_a) estimates for the ENR-25/GP_5–CNT_x hybrid fillers with various CNT loadings

Samples	Heating rate (°C/min)	T_p (°C)	E_a (kJ/mol)	
			Ozawa	Kissinger
Gum ENR-25	2	178.73	120.55	112.72
	10	200.06		
	20	212.46		
	30	220.66		
ENR-25/GP_5	2	177.96	118.61	110.78
	10	199.21		
	20	211.75		
	30	220.61		
ENR-25/GP_5–CNT_1	2	179.15	116.67	108.81
	10	201.54		
	20	213.44		
	30	223.1		
ENR-25/GP_5–CNT_3	2	175.23	116.12	108.34
	10	197.72		
	20	210.12		
	30	218.17		
ENR-25/GP_5–CNT_5	2	177.69	110.68	102.83
	10	202.55		
	20	214.8		
	30	223.66		
ENR-25/GP_5–CNT_7	2	173.24	109.80	102.03
	10	198.39		
	20	210.81		
	30	218.2		

presence of fillers, particularly CNT, promotes the crosslinking reaction of the nanocomposites. This finding aligns well with the decrease in cure time (t_{C90}), scorch time (t_{S1}) and the increase in the cure rate index (CRI) observed in Fig. 5 and Table 3. Also, Table 4 demonstrates that the ENR-25/GP_5–CNT_x composites have lower E_a values compared to ENR-25/GP_5 compounds. This can be attributed to the finer dispersion of CNT in the ENR matrix facilitated by the GP particles, resulting in fewer CNT agglomerates. Additionally, the trend observed in E_a values supports the proposed interactions between the polar functional groups on the filler surfaces and the ENR molecules (Fig. 2).

Mechanical properties

The stress–strain behaviors of gum ENR-25 and its composites filled with 5 phr GP and GP_5–CNT_x hybrid fillers, with varying CNT loadings, are depicted in Fig. 7. Additionally, Table 5 provides a summary of the tensile properties, including tensile strength, elongation at break, 100% modulus, tension set, and hardness of the gum ENR-25 compound, ENR-25/GP_5, and ENR-25/GP5–CNT_x hybrid fillers with different CNT loadings. It can be observed from the data that both gum ENR-25 and ENR-25/GP_5 vulcanizates exhibit strain-induced crystallization at an elongation of approximately 450%. This indicates that the rubber molecules, even with a 25 mol% epoxide group content, can still align themselves due to external forces, leading to strain-induced crystallization [43]. Furthermore, Fig. 7 and Table 5 illustrate that the incorporation of GP in ENR-25/GP_5 and GP–CNT in ENR-25/GP_5–CNT_x results in an increase in Young's modulus (initial slope) and 100% modulus compared to the gum ENR-25 compound. The moduli also demonstrates an increase with higher CNT loadings in ENR-25/GP_5–CNT_x nanocomposites. This can be attributed to the formation of a network and the reinforcing efficiency of the fillers (CNT and GP–CNT hybrid filler) in the ENR matrix, achieved through chemical interactions between the polar functional groups on the filler surfaces and the oxirane rings in ENR molecules [44]. However, it should be noted that an increasing CNT loading leads to a decreasing trend in the tensile strength and elongation at break of ENR-25/GP_5–CNT_x nanocomposites. This can be attributed to the self-aggregation of CNT due to strong particle interactions, resulting in heterogeneous dispersion of CNT particles within the ENR matrix and the formation of larger agglomerations (see in Figs. 3 and 4). Furthermore, the rigid CNT particles hinder the mobility of the ENR molecular networks [21].

Table 5 reveals that the tension set of ENR-25/GP_5 and ENR-25/GP_5–CNT_x increased when fillers were incorporated, in comparison with the gum ENR-25 vulcanizate. Moreover, the tension set values demonstrated an increase with higher CNT loading in ENR-25/GP_5–CNT_x nanocomposites. This indicates a decrease in rubber elasticity or the ability to recover after prolonged extension. The presence of filler networks composed of CNT and GP/CNT hybrid filler restricts the mobility of rubber chains [21]. Additionally, the hardness is another property influenced by the addition of fillers and the increasing CNT loading in hybrid fillers. It is evident from Table 5 that the hardness of all ENR nanocomposites increased as the total amount of filler content in the ENR-25 matrix

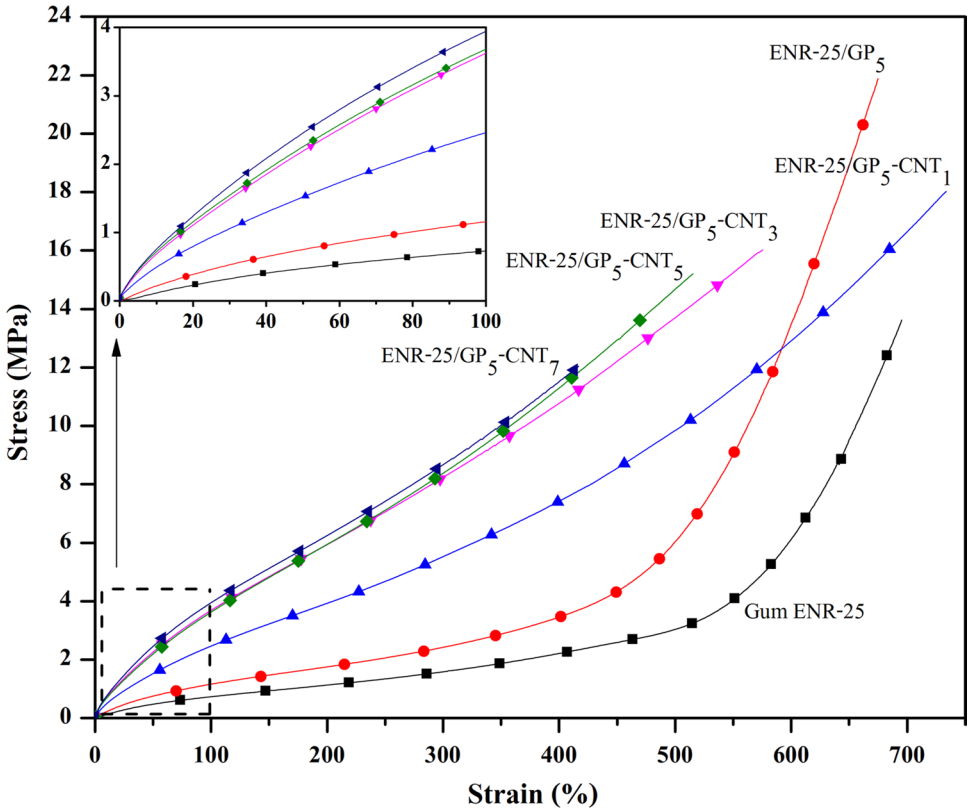

Figure 7 Stress–strain curves for of gum ENR-25 and its filled compounds with 5 phr GP (ENR-25/GP_5) and ENR-25/GP_5–CNT_x hybrid nanocomposites with different CNT loadings at 1, 3, 5, and 7 phr.

Table 5 Mechanical properties in terms of tensile strength, elongation at break, 100% modulus, tension set, and hardness of gum ENR-25 compound, ENR-25/GP_5, and ENR-25/GP_5–CNT_x hybrid fillers with various CNT loadings

Samples	Tensile strength (MPa)	Elongation at break (%)	100% Modulus (MPa)	Tension set (%)	Hardness (Shore A)
Gum ENR-25	13.62 ± 0.27	695.25 ± 25.16	0.73 ± 0.15	0.95 ± 0.23	31.23 ± 0.52
ENR-25/GP_5	20.56 ± 0.23	617.40 ± 20.19	1.12 ± 0.15	1.17 ± 0.54	33.42 ± 0.71
ENR-25/GP_5–CNT_1	18.02 ± 0.18	734.80 ± 22.14	2.45 ± 0.11	1.32 ± 0.19	35.14 ± 1.02
ENR-25/GP_5–CNT_3	16.03 ± 0.14	576.09 ± 19.32	3.62 ± 0.18	1.55 ± 0.74	38.71 ± 0.84
ENR-25/GP_5–CNT_5	15.21 ± 0.20	515.39 ± 19.56	3.68 ± 0.16	1.63 ± 0.66	41.39 ± 0.60
ENR-25/GP_5–CNT_7	12.04 ± 0.19	417.58 ± 21.42	3.94 ± 0.12	1.79 ± 0.58	49.20 ± 0.55

increased. This can be attributed to the incorporation of solid particulates along with the enhanced reinforcing ability of GP and CNT, resulting in higher stiffness in the nanocomposite. Furthermore, it contributes to an increase in the crosslink density of the ENR vulcanizate.

Crosslink density

Table 6 presents the crosslink density of gum ENR-25, ENR-25/GP_5 and ENR-25/GP_5–CNT_x nanocomposites at various CNT loadings (1, 3, 5, and 7 phr). It is

Table 6 Crosslink densities of gum ENR-25 compound, ENR-25/GP_5, and ENR-25/GP_5–CNT_x hybrid fillers with various CNT loadings

Samples	Crosslink density (mol/m^3)
Gum ENR-25	70.25 ± 1.95
ENR-25/GP_5	77.23 ± 1.96
ENR-25/GP_5–CNT_1	85.34 ± 2.30
ENR-25/GP_5–CNT_3	96.69 ± 2.62
ENR-25/GP_5–CNT_5	152.74 ± 2.64
ENR-25/GP_5–CNT_7	189.61 ± 3.12

evident that the ENR/GP composites exhibit higher crosslink densities compared to the gum ENR vulcanizate. This can be attributed to the chemical interaction between the functional groups on the surfaces of GP and ENR (Fig. 2), which leads to strong chemical interactions among the composite components and a higher degree of rubber crosslinking. Additionally, the incorporation of GP_5 and GP_5–CNT_x hybrid fillers results in increased crosslink density, which correlates well with the observed increase in torque difference (M_H–M_L) as shown in Table 3. The increase in crosslink density also corresponds to higher hardness and modulus values in the ENR composites, as indicated in Table 5. This relationship is consistent with the decrease in elongation at break due to the restricted mobility of the crosslink joints within the rubber networks. Interestingly, the crosslink density increases with the addition of fillers and increasing CNT loadings. However, this contradicts the decreasing trend observed in tensile strength (Table 3). One possible explanation for this discrepancy is the formation of larger filler agglomerates with increasing filler loadings, as depicted in Figs. 3 and 4. These agglomerates can act as stress concentration points, leading to a reduction in the overall tensile strength of the composites. Furthermore, a high crosslink density in rubber vulcanizates has a significant impact on reducing strain-induced crystallization (SIC), which in turn restricts the orientation of rubber chains. As a consequence, this leads to a decrease in tensile strength [45].

Degree of reinforcement

The degree of filler reinforcement in the rubber matrix has been assessed using the Kraus equation, as follows [46]:

$$\frac{V_{r0}}{V_{rf}} = 1 - m\left(\frac{f}{1-f}\right) \tag{11}$$

where V_{r0} and V_{rf} represent the volume fractions of rubber in the gum vulcanizate and in filler–filled swollen sample, respectively. f denotes the volume fraction of the filler, and m is defined as the filler–polymer interaction parameter ($m = 1.17$).

Figure 8 shows the Kraus plot (depicting V_{r0}/V_{rf} as function of $f/(1-f)$)) for ENR-25/GP_5 and ENR-25/GP_5–CNT_x hybrid nanocomposites with varying CNT loadings. The pronounced decrease in V_{r0}/V_{rf} values is clearly observed with the increasing CNT loadings. In accordance with Kraus theory, the reinforcement effect is expected to yield a steeper negative slope [47],

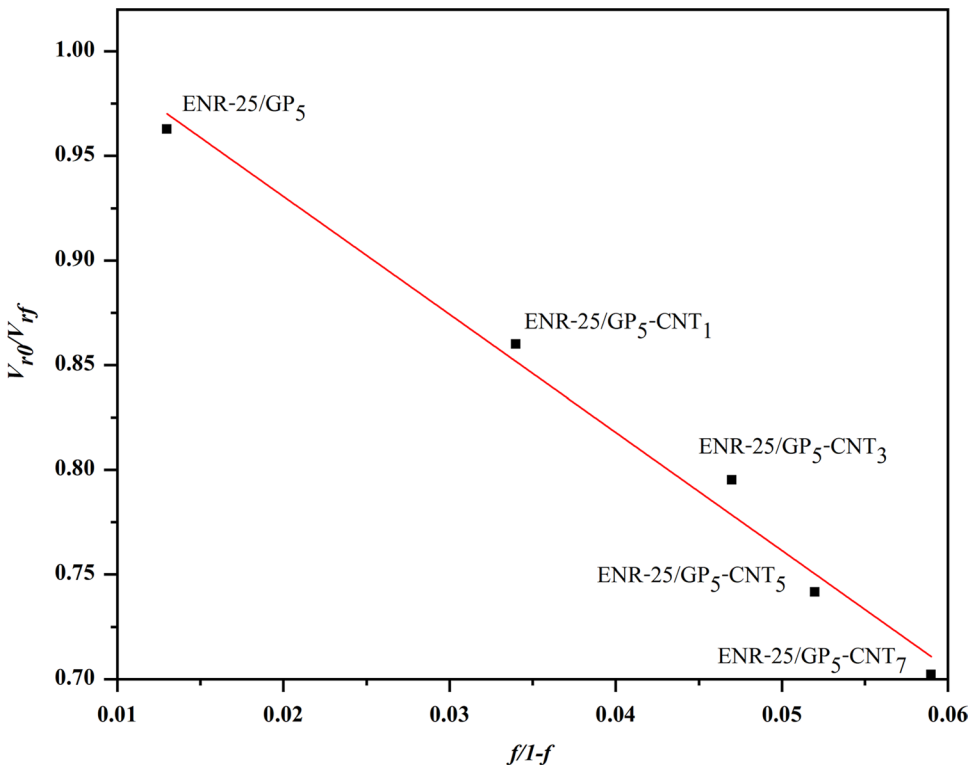

Figure 8 Kraus plot of ENR-25/GP_5 and ENR-25/GP_5–CNT_x hybrid nanocomposites with different CNT loadings at 1, 3, 5, and 7 phr.

which aligns with our findings in Fig. 8. Notably, the increment in slope corresponds to the increasing CNT content in ENR-25/GP_5–CNT_x hybrid nanocomposites. This observation confirms the establishment of an effective interface between the carbon nanofiller and the ENR matrix, preventing solvent diffusion and thus resulting in a higher degree of reinforcement. Consequently, the Kraus plot corresponds with the crosslink density measurements derived from the Flory–Rehner theory (Table 6).

Payne effect

Figure 9 shows storage modulus as a function of strain amplitude for gum ENR-25, ENR-25/GP_5 compounds and ENR-25/GP_5–CNT_x hybrid composites with various CNT loadings. It is clearly seen that the gum ENR-25 compound shows the lowest storage modulus (G') with more or less strain independent or absence of the Payne effect. In contrast, the incorporation of 5 phr GP and GP–CNT_x hybrid filler caused significantly increase in the storage modulus

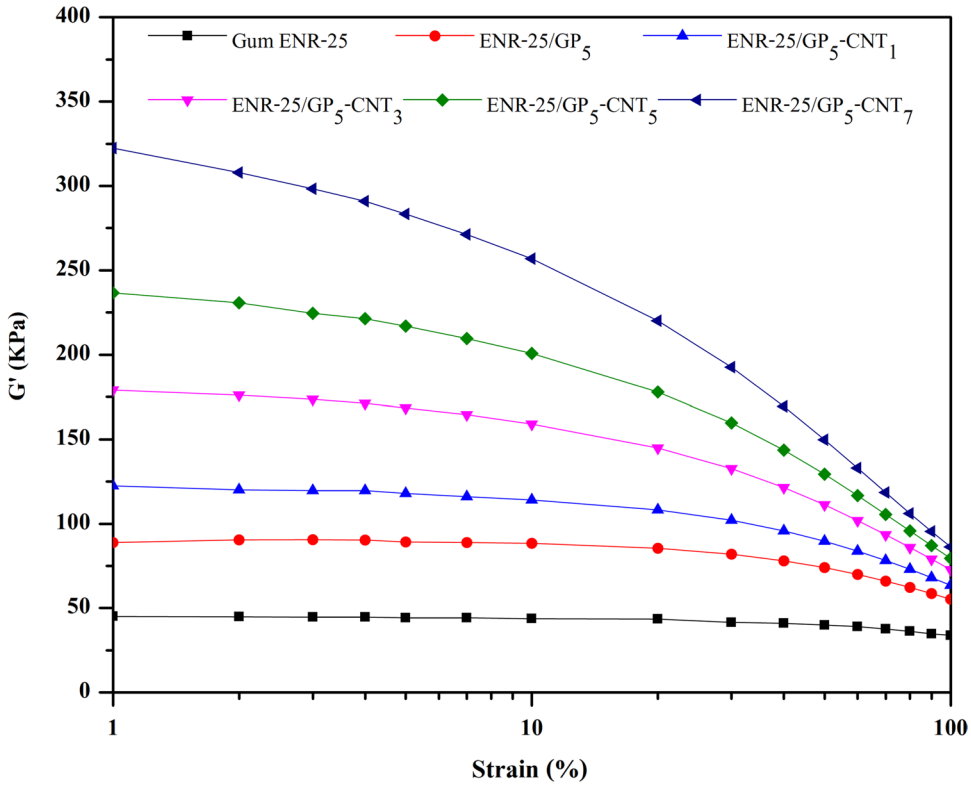

Figure 9 Relationship between storage modulus and strain amplitude of gum ENR-25, ENR-25 filled with 5 phr GP (ENR-25/GP_5) and ENR-25/GP_5–CNT_x hybrid nanocomposites with different CNT loadings at 1, 3, 5, and 7 phr.

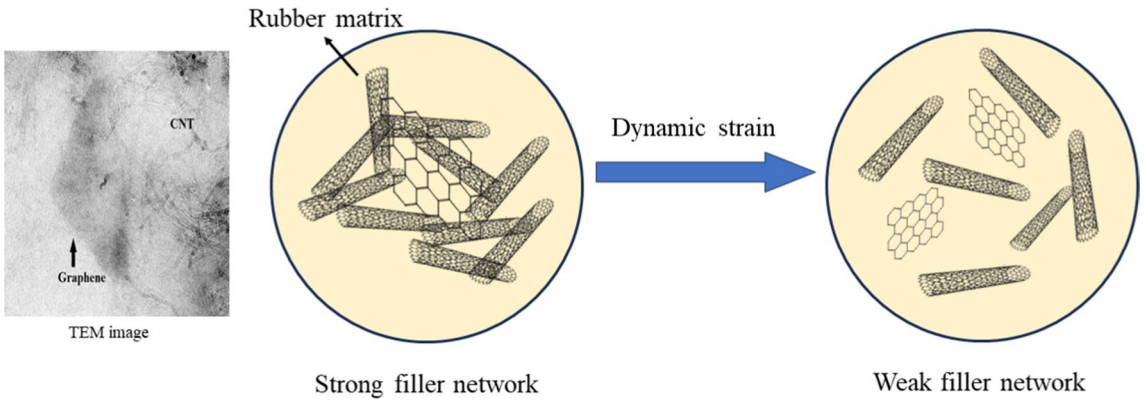

Figure 10 Schematic representation of the breakdown of filler network under dynamic strain.

Table 7 Storage moduli (G') of gum ENR, and their filled compounds with GP and GP/CNT_x hybrid fillers at very low ($G'_{0.56}$) and high (G'_{100}) strain amplitudes, as well as their difference ($\Delta G'$)

Samples	$G'_{0.56}$	G'_{100}	$\Delta G'$	$\%\Delta G'$	Payne effect (%)
Gum ENR-25	46.01	33.40	12.61	37.75	–
ENR-25/GP_5	88.21	55.70	32.51	58.37	20.61
ENR-25/GP_5–CNT_1	123.41	63.14	60.27	95.45	57.70
ENR-25/GP_5–CNT_3	177.65	71.22	106.43	149.44	111.68
ENR-25/GP_5–CNT_5	237.63	77.54	160.09	206.46	168.71
ENR-25/GP_5–CNT_7	321.72	86.10	235.62	273.66	235.90

and significantly increase in G' in ENR-25/GP_5–CNT_x compounds with increasing CNT loadings. This might be due to the stronger filler–filler interaction of hybrid filler [30]. Furthermore, the abrupt decrease in storage modulus of different rubber compounds is clearly seen after strain amplitude higher than 10%. That may cause by the collapse or breaking up of filler networks in the rubber compound at large strain amplitude [48, 49], as a schematic representation of the filler network's breakdown under dynamic strain illustrated in Fig. 10. Additionally, the Payne effect is observed due to hydrodynamic reinforcement and interactions between fillers [50]. Also, Table 7 illustrates storage moduli (G') of gum ENR and their filled compounds with GP and GP/CNT_x hybrid fillers at very low ($G'0.56$) and high ($G'100$) strain amplitudes, as well as their difference ($\Delta G'$). It can be seen that the ENR-25/GP_5 showed a Payne effect at 20.61%, while the ENR-25/GP_5–CNT_x with 1–7 phr of CNT had the higher Payne effect according their CNT loadings at 57.70, 111.68, 168.71, and 235.90%, respectively. This is due to higher energy loss in terms of strain amplitude during breaking up of strong filler hybrid networks along with their agglomeration [51]. This correlates well with the morphological properties described in Figs. 3 and 4.

Electrical properties

Figure 11 illustrates the electrical conductivity as a function of frequency for gum ENR-25, ENR-25/GP_5,

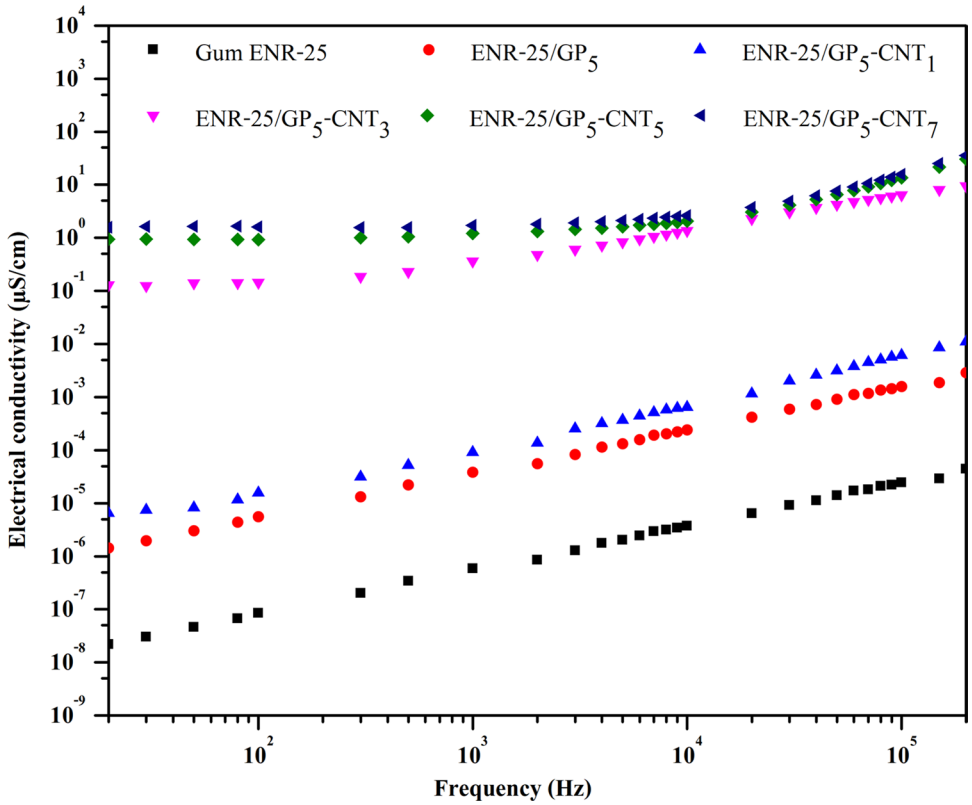

Figure 11 Electrical conductivity of gum ENR-25, ENR-25 filled with 5 phr GP (ENR-25/GP_5) and ENR-25/GP_5–CNT_x hybrid nanocomposites with different CNT loadings at 1, 3, 5, and 7 phr.

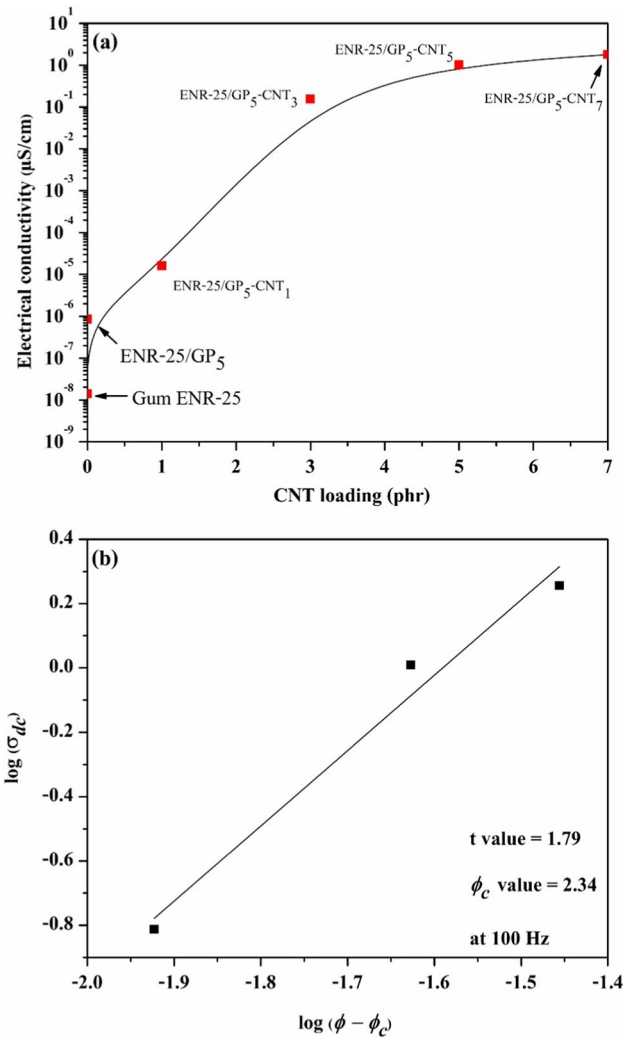

Figure 12 **a** Relationship between electrical conductivity and CNT loadings for GP_5/CNT-filled ENR-25 nanocomposites with different CNT loadings, and **b** log (σ_{dc}) versus log (ϕ–ϕ_c).

and ENR-25/GP_5–CNT_x hybrid nanocomposites with varying CNT loadings at 1, 3, 5, and 7 phr. It is evident that the electrical conductivity increases with the incorporation of filler and increasing CNT loadings. Moreover, the gum ENR vulcanizate as well as its nanocomposites with GP (ENR/GP_5) and ENR-25/GP_5–CNT_1 exhibits a significant increase in electrical conductivity with increasing frequency. However, the ENR-25/GP_5–CNT_x composites with higher CNT loadings (i.e., 3, 5, and 7 phr) demonstrate a marginal increasing trend of electrical conductivity as frequency increases, with slightly steeper curves beyond frequencies of 1×10^5 Hz. This phenomenon can be attributed to the flow of electrons within the filler networks, at the interface between the hybrid fillers, and within the polymer matrix [52]. Specifically, the ENR-25/GP_5–CNT_1 shows conductivity below the critical filler loading or percolation threshold concentration (PTC). However, as the CNT loading exceeds 1 phr, a conductive filler network is formed, leading to a sudden increase in electrical conductivity due to the establishment of continuous conductive paths through the filler networks [53]. This is supported by the relationship between electrical conductivity at a frequency of 100 Hz and CNT loadings, as depicted in Fig. 12a. It is evident that the electrical conductivity increases significantly when the CNT loading increases from 1 to 3 phr, while a marginal increase in conductivity is observed within the CNT loading range of 3 to 5 phr. This behavior indicates that the filler content above percolation threshold concentration. To determine a precise PCT for this type of nanocomposite, the fundamental percolation theory was applied to estimate the PCT level using Eqs. (12) and (13) [54]. The results are presented in Fig. 12b.

$$\sigma_{dc} = \kappa\left(\phi - \phi_c\right)^t \quad \text{for} \quad \phi > \phi_c \tag{12}$$

$$\log(\sigma_{dc}) = \log\kappa + t \cdot \log\left(\phi - \phi_c\right) \tag{13}$$

where σ_{dc} is the electrical conductivity (μS/cm), κ is a constant parameter, ϕ is the volume fraction of filler, ϕ_c is the critical loading (volume fraction at percolation threshold), and t is a critical exponent.

From the plot in Fig. 12b, the critical loading level of the percolation threshold concentration (ϕ_c) was determined to be 2.34 phr, and the t value was calculated to be 1.79. Typically, the t value is used to assess the network structure of rubber composites. A t value ranging from 1.6 to 2.0 suggests a three-dimensional filler network, while t values below 1.6 indicate a two-dimensional network [55]. Therefore, the ENR-25/GP_5–CNT_x nanocomposites exhibit a fully three-dimensional filler network (t = 1.79) at a CNT loading of 2.34 phr, indicating a fully conductive nature of the ENR hybrid composites. Consequently, the critical CNT concentration of 2.34 phr transforms the ENR vulcanizate from an insulating material to a conducting material [56], due to the formation of an infinite conductive filler network within the ENR matrix after the addition of 2.34 phr of CNT to the ENR-25/GP_5/CNT_x hybrid composites.

Therefore, the increasing electrical conductivity–frequency curves in Fig. 11 and the conductivity

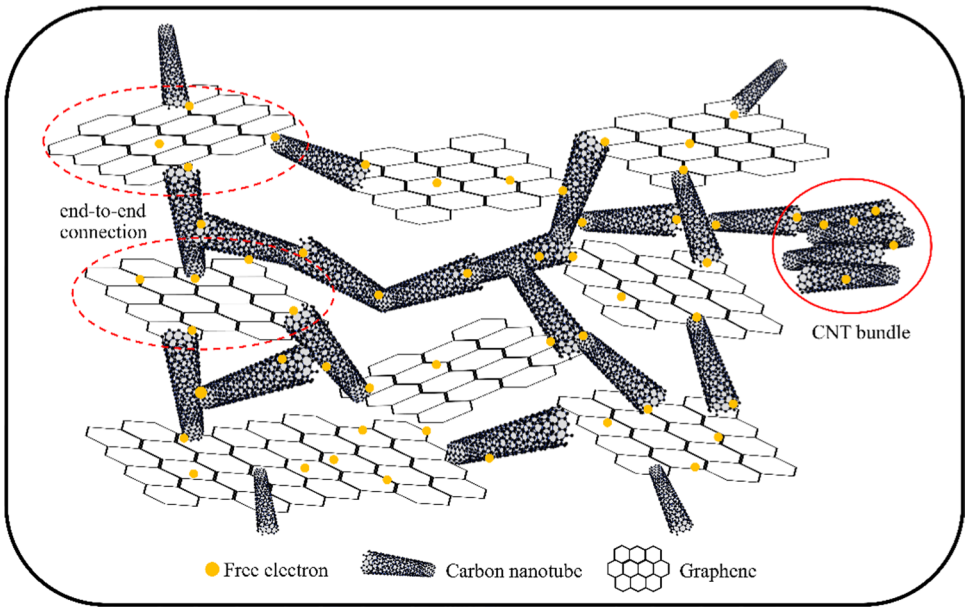

Figure 13 A proposed model for formation of GP and CNT hybrid filler networks in ENR matrix.

at a given frequency shown in Fig. 12, observed when 5 phr of GP is incorporated into ENR-25 (i.e., ENR-25/GP_5), as well as the increasing CNT loadings in the ENR-25/GP_5–CNT_x hybrid composites, can be attributed to the movement of free electrons within the structures of GP and CNT. These electrons are capable of traversing the ENR matrix [57]. Additionally, the high electrical conductivity of both GP and CNT, which possess similar graphitic structures consisting of sp^2-hybridized carbon atoms, contributes to the enhanced electrical conductivity. This results in the formation of pathways for electron movement along the networks of GP and CNT, facilitated by Van der Waals forces, dipole–dipole interactions, and π–π interactions [36], as a proposed model in Fig. 13. This is a significant factor contributing to the higher electrical conductivity exhibited by ENR-25/GP_5–CNT_x compared to gum ENR-25 and ENR-25/GP_5 composites.

Conclusion

ENR-25/GP_5–CNT_x hybrid nanocomposites were prepared by incorporating various CNT loadings of 1, 3, 5, and 7 phr. The FTIR and TEM results revealed the occurrence of chemical reactions between the polar functional groups in the ENR molecules and the surfaces of GP–CNT. Additionally, the hybridization of GP and CNT was found to improve multiple properties of the ENR composites. Firstly, the cure properties of the composites were enhanced, as evidenced by a decrease in the activation energy of vulcanization. This reduction in activation energy suggests that loading CNT in the hybrid fillers leads to a shorter cure time. Moreover, the incorporation of CNT resulted in increased modulus and hardness, indicating reinforcement of the composites. These findings were consistent with the crosslink density measurements obtained from the Flory–Rehner theory. This effect can be attributed to the formation of end-to-end connections between certain parts of the CNT and the GP, leading to the establishment of a three-dimensional filler network with strong interaction among the components. The observed increase in electrical conductivity and the presence of a low percolation threshold concentration at 2.34 phr of CNT indicate that the hybrid composites exhibit conductive properties.

Acknowledgements

The authors would like to acknowledge financial support by the National Research Council of Thailand (NRCT) under Grant No. NRCT-RGJ63019-159. Moreover, Faculty of Science and Industrial Technology, Prince of Songkla University Surat Thani campus and University of Applied Science, Osnabrück, Germany are highly acknowledged for access to facilities and equipment.

Author contributions

TS was performed investigation, analysis, and wrote the original draft. SP1 was managed the data and contributed to writing the review. MS was provided supervision, supplied laboratory facilities, and confirmed the results. SP2 was interpreted the findings. CN was supervised the project, validated the results, reviewed and edited the manuscript, and contributed to its completion.

Data and code availability

In response to legitimate requests, the authors will provide relevant data.

Declarations

Conflict of interest The authors declare that they have no conflict of interest.

References

[1] Ruksakulpiwat C, Nuasaen S, Poonsawat C, Khansawai P (2008) Synthesis and modification of epoxidized natural rubber from natural rubber latex. Adv Mat Res 47:734–737. https://doi.org/10.4028/www.scientific.net/AMR.47-50.734

[2] Baker C, Gelling I (1987) Epoxidized natural rubber. Developments in rubber technology-4. Elsevier, New York. https://doi.org/10.1007/978-94-009-3435-1_3

[3] Nakaramontri Y, Nakason C, Kummerlöwe C, Vennemann N (2015) Influence of modified natural rubber on properties of natural rubber–carbon nanotube composites. Rubber Chem Technol 88:199–218. https://doi.org/10.5254/rct.14.85949

[4] Hong S-G, Chan C-K (2004) The curing behaviors of the epoxy/dicyanamide system modified with epoxidized natural rubber. Thermochim Acta 417:99–106. https://doi.org/10.1016/j.tca.2003.12.015

[5] Srirachya N, Kobayashi T, Boonkerd K (2017) An alternative crosslinking of epoxidized natural rubber with maleic anhydride. Key Eng Mater 748:84–90. https://doi.org/10.4028/www.scientific.net/KEM.748.84

[6] Pire M, Norvez S, Iliopoulos I, Le Rossignol B, Leibler L (2010) Epoxidized natural rubber/dicarboxylic acid self-vulcanized blends. Polymer 51:5903–5909. https://doi.org/10.1016/j.polymer.2010.10.023

[7] Fan Y, Fowler GD, Zhao M (2020) The past, present and future of carbon black as a rubber reinforcing filler: a review. J Clean Prod 247:119115. https://doi.org/10.1016/j.jclepro.2019.119115

[8] Das A, Kasaliwal GR, Jurk R, Boldt R, Fischer D, Stöckelhuber KW, Heinrich G (2012) Rubber composites based on graphene nanoplatelets, expanded graphite, carbon nanotubes and their combination: a comparative study. Compos Sci Technol 72:1961–1967. https://doi.org/10.1016/j.compscitech.2012.09.005

[9] Guo H, Ji P, Halász IZ et al (2020) Enhanced fatigue and durability properties of natural rubber composites reinforced with carbon nanotubes and graphene oxide. Materials 13:5746. https://doi.org/10.3390/ma13245746

[10] Pradhan B, Srivastava SK (2014) Synergistic effect of three-dimensional multi-walled carbon nanotube–graphene nanofiller in enhancing the mechanical and thermal properties of high-performance silicone rubber. Polym Int 63:1219–1228. https://doi.org/10.1002/pi.4627

[11] Yang B, Wang S, Song Z, Liu L, Li H, Li Y (2021) Molecular dynamics study on the reinforcing effect of incorporation of graphene/carbon nanotubes on the mechanical properties of swelling rubber. Polym Test 102:107337. https://doi.org/10.1016/j.polymertesting.2021.107337

[12] Park S, Ruoff RS (2009) Chemical methods for the production of graphenes. Nat Nanotechnol 4:217–224. https://doi.org/10.1038/nnano.2009.58

[13] Bruna M, Borini S (2009) Optical constants of graphene layers in the visible range. Appl Phys Lett 94:031901. https://doi.org/10.1063/1.3073717

[14] Hwangbo Y, Lee C-K, Kim S-M et al (2014) Fracture characteristics of monolayer CVD-graphene. Sci Rep 4:4439. https://doi.org/10.1038/srep04439

[15] Martins LG, Song Y, Zeng T, Dresselhaus MS, Kong J, Araujo PT (2013) Direct transfer of graphene onto flexible substrates. Proc Natl Acad Sci 110:17762–17767. https://doi.org/10.1073/pnas.1306508110

[16] Lv H, Wu H, Liu J et al (2013) High carrier mobility in suspended-channel graphene field effect transistors. Appl Phys Lett 103:193102. https://doi.org/10.1063/1.4828835

[17] Ghosh D, Calizo I, Teweldebrhan D et al (2008) Extremely high thermal conductivity of graphene: prospects for thermal management applications in nanoelectronic circuits. Appl Phys Lett 92:151911. https://doi.org/10.1063/1.2907977

[18] Worsley MA, Pauzauskie PJ, Olson TY, Biener J, Satcher JH Jr, Baumann TF (2010) Synthesis of graphene aerogel with high electrical conductivity. J Am Chem Soc 132:14067–14069. https://doi.org/10.1021/ja1072299

[19] Sa K, Mahakul PC, Subramanyam B, Raiguru J, Das S, Alam I, Mahanandia P (2018) Effect of reduced graphene oxide-carbon nanotubes hybrid nanofillers in mechanical properties of polymer nanocomposites. IOP Conf Ser Mater Sci Eng 338:012055. https://doi.org/10.1088/1757-899X/338/1/012055

[20] Zulhairun AK, Abdullah MS, Ismail AF, Goh PS (2019) Graphene and CNT technology. In: Basile A, Curcio E, Inamuddin (eds) Current trends and future developments on (bio-) membranes. Elsevier, New York, pp 3–26. https://doi.org/10.1016/B978-0-12-813551-8.00001-2

[21] Krainoi A, Kummerlöwe C, Nakaramontri Y, Vennemann N, Pichaiyut S, Wisunthorn S, Nakason C (2018) Influence of critical carbon nanotube loading on mechanical and electrical properties of epoxidized natural rubber nanocomposites. Polym Test 66:122–136. https://doi.org/10.1016/j.polymertesting.2018.01.003

[22] Liu Y, Huang J, Zhou F, Ni L, Shen Y, Liu W, Meng F (2021) A mini-review of three-dimensional network topological structure nanocomposites: preparation and mechanical properties. Nanotechnol Rev 10:1425–1437. https://doi.org/10.1515/ntrev-2021-0094

[23] Szeluga U, Kumanek B, Trzebicka B (2015) Synergy in hybrid polymer/nanocarbon composites. A review. Compos A Appl Sci Manuf 73:204–231. https://doi.org/10.1016/j.compositesa.2015.02.021

[24] Nam K-H, Yu J, You N-H, Han H, Ku B-C (2017) Synergistic toughening of polymer nanocomposites by hydrogen-bond assisted three-dimensional network of functionalized graphene oxide and carbon nanotubes. Compos Sci Technol 149:228–234. https://doi.org/10.1016/j.compscitech.2017.06.025

[25] Siriwas T, Pichaiyut S, Susoff M, Petersen S, Nakason C (2023) Graphene-filled natural rubber nanocomposites: influence of the composition on curing, morphological, mechanical, and electrical properties. Express Polym Lett. https://doi.org/10.3144/expresspolymlett.2023.61

[26] Yangthong H, Wisunthorn S, Pichaiyut S, Nakason C (2019) Novel epoxidized natural rubber composites with geopolymers from fly ash waste. Waste Manag 87:148–160. https://doi.org/10.1016/j.wasman.2019.02.013

[27] Flory PJ, Rehner J Jr (1943) Statistical mechanics of cross-linked polymer networks I. Rubberlike elasticity. J Chem Phys 11:512–520. https://doi.org/10.1063/1.1723791

[28] Flory PJ (1941) Molecular size distribution in three dimensional polymers. II. Trifunctional branching units. J Am Chem Soc 63:3091–3096. https://doi.org/10.1021/ja01856a062

[29] Ojogbo E, Tzoganakis C, Mekonnen TH (2021) Effect of extrusion, batch-mixing, and co-coagulation on the dispersion of CNCs in natural rubber-CNC nanocomposites. Compos A Appl Sci Manuf 149:106580. https://doi.org/10.1016/j.compositesa.2021.106580

[30] Payne A (1965) Effect of dispersion on the dynamic properties of filler-loaded rubbers. J Appl Polym Sci 9:2273–2284. https://doi.org/10.1002/app.1965.070090619

[31] Krainoi A, Kummerlöwe C, Nakaramontri Y et al (2020) Novel natural rubber composites based on silver nanoparticles and carbon nanotubes hybrid filler. Polym Compos 41:443–458. https://doi.org/10.1002/pc.25378

[32] Du F, Fischer JE, Winey KI (2003) Coagulation method for preparing single-walled carbon nanotube/poly (methyl methacrylate) composites and their modulus, electrical conductivity, and thermal stability. J Polym Sci B Polym Phys 41:3333–3338. https://doi.org/10.1002/polb.10701

[33] Omonov TS, Curtis JM (2016) Plant oil-based epoxy intermediates for polymers. In: Madbouly SA, Zhang C, Kessler MR (eds) Bio-based plant oil polymers and composites. Elsevier, New York, pp 99–125. https://doi.org/10.1016/B978-0-323-35833-0.00007-4

[34] Coates J (2000) Interpretation of infrared spectra, a practical approach. In: Meyers RA (ed) Encyclopedia of analytical chemistry. Wiley, Hoboken, pp 10815–10837. https://doi.org/10.1002/9780470027318.a5606

[35] Krainoi A, Kummerlöwe C, Vennemann N, Nakaramontri Y, Pichaiyut S, Nakason C (2019) Effect of carbon nanotubes decorated with silver nanoparticles as hybrid filler on properties of natural rubber nanocomposites. J Appl Polym Sci 136:47281. https://doi.org/10.1002/app.47281

[36] Kitisavetjit W, Nakaramontri Y, Pichaiyut S, Wisunthorn S, Nakason C, Kiatkamjornwong S (2021) Influences of carbon nanotubes and graphite hybrid filler on properties of natural rubber nanocomposites. Polym Test 93:106981. https://doi.org/10.1016/j.polymertesting.2020.106981

[37] Yazid H, Anwar UA, Zaubidah AS et al (2022) A combined method to probe the behaviour of the filler in polymer blend nanocomposites via X-ray diffraction and thermal measurement. Nanostruct Nanoobj 32:100906. https://doi.org/10.1016/j.nanoso.2022.100906

[38] Kim P, Shi L, Majumdar A, McEuen PL (2001) Thermal transport measurements of individual multiwalled nanotubes. Phys Rev Lett 87:215502. https://doi.org/10.1103/PhysRevLett.87.215502

[39] Nakaramontri Y, Kummerlöwe C, Nakason C, Vennemann N (2014) Effect of modified natural rubber and functionalization of carbon nanotubes on properties of natural rubber

composites. Adv Mat Res 844:301–304. https://doi.org/10.4028/www.scientific.net/AMR.844.301

[40] Hernández M, del Mar BM, Verdejo R, Ezquerra TA, López-Manchado MA (2012) Overall performance of natural rubber/graphene nanocomposites. Compos Sci Technol 73:40–46. https://doi.org/10.1016/j.compscitech.2012.08.012

[41] Pongdong W, Nakason C, Kummerlöwe C, Vennemann N (2015) Influence of filler from a renewable resource and silane coupling agent on the properties of epoxidized natural rubber vulcanizates. J Chem. https://doi.org/10.1155/2015/796459

[42] Ozawa T (1965) A new method of analyzing thermogravimetric data. Bull Chem Soc Jpn 38:1881–1886. https://doi.org/10.1246/bcsj.38.1881

[43] Zhang X, Niu K, Song W, Yan S, Zhao X, Lu Y, Zhang L (2019) The effect of epoxidation on strain-induced crystallization of epoxidized natural rubber. Macromol Rapid Commun 40:1900042. https://doi.org/10.1002/marc.201900042

[44] Damampai K, Pichaiyut S, Dasa A, Nakason C (2022) Internal polymerization of epoxy group of epoxidized natural rubber by ferric chloride filled with carbon nanotubes: mechanical, morphological, thermal and electrical properties of rubber vulcanizates. Express Polym Lett 16:812–826. https://doi.org/10.3144/expresspolymlett.2022.60

[45] Chenal J-M, Gauthier C, Chazeau L, Guy L, Bomal Y (2007) Parameters governing strain induced crystallization in filled natural rubber. Polymer 48:6893–6901. https://doi.org/10.1016/j.polymer.2007.09.023

[46] Kraus G (1963) Swelling of filler-reinforced vulcanizates. J Appl Polym Sci 7:861–871. https://doi.org/10.1002/app.1963.070070306

[47] Yaragalla S, Meera A, Kalarikkal N, Thomas S (2015) Chemistry associated with natural rubber–graphene nanocomposites and its effect on physical and structural properties. Ind Crops Prod 74:792–802. https://doi.org/10.1016/j.indcrop.2015.05.079

[48] Yang G, Liao Z, Yang Z, Tang Z, Guo B (2015) Effects of substitution for carbon black with graphene oxide or graphene on the morphology and performance of natural rubber/carbon black composites. J Appl Polym Sci. https://doi.org/10.1002/app.41832

[49] Meera A, Said S, Grohens Y, Thomas S (2009) Nonlinear viscoelastic behavior of silica-filled natural rubber nanocomposites. J Phys Chem C 113:17997–18002. https://doi.org/10.1021/jp9020118

[50] Ponnamma D, Sadasivuni KK, Strankowski M, Guo Q, Thomas S (2013) Synergistic effect of multi walled carbon nanotubes and reduced graphene oxides in natural rubber for sensing application. Soft Matter 9:10343–10353. https://doi.org/10.1039/c3sm51978c

[51] Dong B, Liu C, Lu Y, Wu Y (2015) Synergistic effects of carbon nanotubes and carbon black on the fracture and fatigue resistance of natural rubber composites. J Appl Polym Sci. https://doi.org/10.1002/app.42075

[52] Vavouliotis A, Fiamegou E, Karapappas P, Psarras G, Kostopoulos V (2010) DC and AC conductivity in epoxy resin/multiwall carbon nanotubes percolative system. Polym Compos 31:1874–1880. https://doi.org/10.1002/pc.20981

[53] Dalmas F, Dendievel R, Chazeau L, Cavaillé J-Y, Gauthier C (2006) Carbon nanotube-filled polymer composites. Numerical simulation of electrical conductivity in three-dimensional entangled fibrous networks. Acta Mater 54:2923–2931. https://doi.org/10.1016/j.actamat.2006.02.028

[54] Ma P-C, Siddiqui NA, Marom G, Kim J-K (2010) Dispersion and functionalization of carbon nanotubes for polymer-based nanocomposites: a review. Compos A Appl Sci Manuf 41:1345–1367. https://doi.org/10.1016/j.compositesa.2010.07.003

[55] Bhattacharyya S, Sinturel C, Bahloul O, Saboungi M-L, Thomas S, Salvetat J-P (2008) Improving reinforcement of natural rubber by networking of activated carbon nanotubes. Carbon 46:1037–1045. https://doi.org/10.1016/j.carbon.2008.03.011

[56] Sohi N, Bhadra S, Khastgir D (2011) The effect of different carbon fillers on the electrical conductivity of ethylene vinyl acetate copolymer-based composites and the applicability of different conductivity models. Carbon 49:1349–1361. https://doi.org/10.1016/j.carbon.2010.12.001

[57] Ravindran AR, Feng C, Huang S, Wang Y, Zhao Z, Yang J (2018) Effects of graphene nanoplatelet size and surface area on the AC electrical conductivity and dielectric constant of epoxy nanocomposites. Polymers 10:477. https://doi.org/10.3390/polym10050477